Biosci. Rep. (2016) / **36** / art:e00294 / doi 10.1042/BSR20150203

Original Paper

OPEN ACCESS

Biochemical and structural characterization of polyphosphate kinase 2 from the intracellular pathogen *Francisella tularensis*

Laura E. Batten*, Alice E. Parnell*, Neil J. Wells*, Amber L. Murch*†, Petra C. F. Oyston†† and Peter L. Roach*‡[1]

*Department of Chemistry, University of Southampton, Southampton, SO17 1BJ, U.K.
†Defence Science and Technology Laboratory, Porton Down, Salisbury, SP4 OJQ, U.K.
‡Institute for Life Sciences, University of Southampton, Southampton, SO17 1BJ, U.K.

Synopsis

The metabolism of polyphosphate is important for the virulence of a wide range of pathogenic bacteria and the enzymes of polyphosphate metabolism have been proposed as an anti-bacterial target. In the intracellular pathogen *Francisella tularensis*, the product of the gene FTT1564 has been identified as a polyphosphate kinase from the polyphosphate kinase 2 (PPK2) family. The isogenic deletion mutant was defective for intracellular growth in macrophages and was attenuated in mice, indicating an important role for polyphosphate in the virulence of *Francisella*. Herein, we report the biochemical and structural characterization of *F. tularensis* polyphosphate kinase (*Ft*PPK2) with a view to characterizing the enzyme as a novel target for inhibitors. Using an HPLC-based activity assay, the substrate specificity of *Ft*PPK2 was found to include purine but not pyrimidine nts. The activity was also measured using ^{31}P-NMR. *Ft*PPK2 has been crystallized and the structure determined to 2.23 Å (1 Å = 0.1 nm) resolution. The structure consists of a six-stranded parallel β-sheet surrounded by 12 α-helices, with a high degree of similarity to other members of the PPK2 family and the thymidylate kinase superfamily. Residues proposed to be important for substrate binding and catalysis have been identified in the structure, including a lid-loop and the conserved Walker A and B motifs. The ΔFTT1564 strain showed significantly increased sensitivity to a range of antibiotics in a manner independent of the mode of action of the antibiotic. This combination of biochemical, structural and microbiological data provide a sound foundation for future studies targeting the development of PPK2 small molecule inhibitors.

Key words: antibiotic sensitivity, enzyme kinetics, *Francisella tularensis*, kinase, polyphosphate, X-ray crystallography

Cite this article as: Bioscience Reports (2015) **36**, e00294, doi:10.1042/BSR20150203

INTRODUCTION

Polyphosphate is an inorganic polymer which may extend to hundreds of phosphate residues linked as phospho-anhydrides and has been reported in cells from every domain of life [1]. At one time, polyphosphate was regarded as a 'molecular fossil' [2], providing a prebiotic source of phosphoanhydride equivalents [2] and without a precise described function, but recent discoveries have made it increasingly clear than nothing could be further from the truth. In eukaryotes, polyphosphate has been identified in a range of subcellular organelles [3] and has regulatory roles in a wide range of processes [4–7]. Polyphosphate is ubiquitous in prokaryotes [8], contributing to metabolic regulation during growth and development and contributing to the regulatory network that controls the response to stress and nutrient starvation [9–13]. The importance of polyphosphate to bacterial survival [8,9,14] and, in particular, it's correlation to the virulence of a wide spectrum of pathogens [14–17], has led to the proposal that enzymes from polyphosphate metabolism are potential therapeutic targets for anti-bacterial chemotherapy [14,18].

For the assembly of polyphosphate chains, three subclasses of bacterial polyphosphate kinases have been identified (Scheme 1). The polyphosphate kinase 1 (PPK1) family is found in the

Abbreviations: AMP-PNP, adenylyl-imidodiphosphate; BCGA, blood cysteine glucose agar; CDC, Centers for Disease Control and Prevention; DMHA, dimethylhexylamine; *Ft, Francisella tularensis* subspecies *tularensis* SCHU S4; *Ft*PPK2, *F. tularensis* polyphosphate kinase; IP, ion pairing; ITC, isothermal titration calorimetry; MES, 2-(N-morpholino)ethanesulfonic acid; NMP, nucleotide monophosphate; PPK2, polyphosphate kinase 2; Ppx, polyphosphatase; *Sm, Sinorhizobium meliloti*; 2YT, yeast extract and tryptone media.

[1] To whom correspondence should be addressed (email plr2@soton.ac.uk).

Scheme 1 **Reaction scheme for the three classes of polyphosphate kinases, PPK1, PPK2 and PPK3, indicating observed substrate specificity of the different enzyme classes**

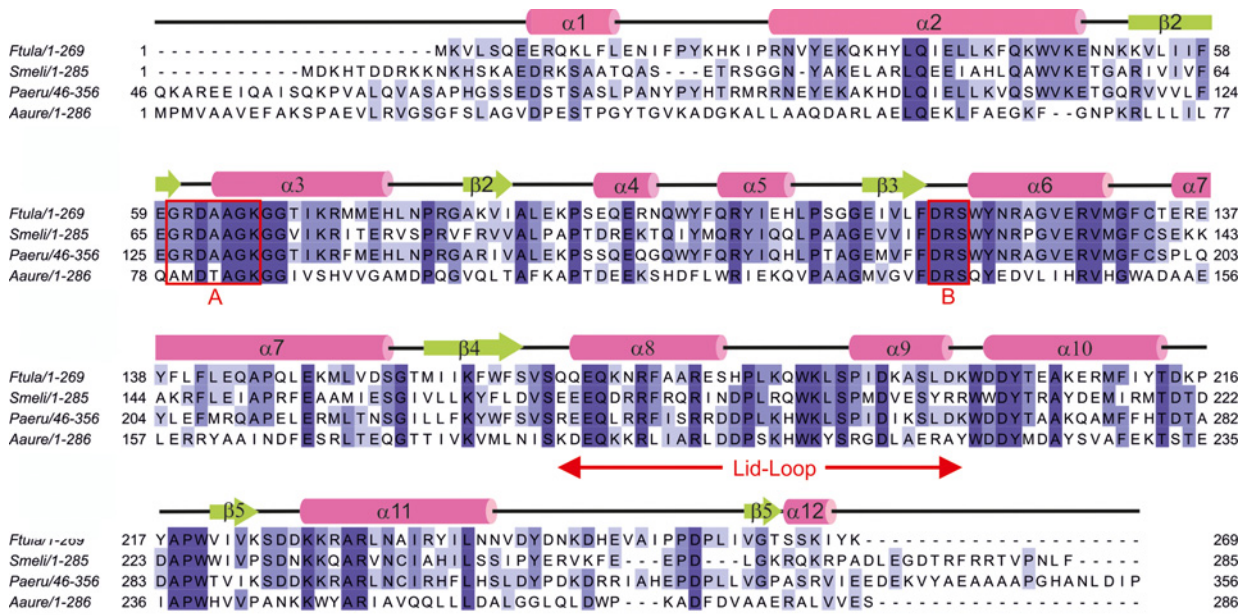

Figure 1 **Alignment of PPK2 sequences from *F. tularensis* (labelled *Ftula*, accession code YP_170487.1, PDB code 4YEG), *P. aeruginosa* (*Paeru*, NP_248831, 3CZP), *S. meliloti* (*Smeli*, NP_384613, 3CZQ) and *A. aurescens* (*Aaure*, YP_949739.1, 3RHF)**

Residues are coloured by degree of conservation. Elements of secondary structure are taken from the *F. tularensis* structure (α-helices in pink, β-sheets in green). The Walker A and B motifs of PPK2 identified by Nocek et al. [23] are boxed in red. The unaligned N-terminal 45 residues of *Pa*PPK2 are omitted.

majority of bacterial species [19] and constitutes the principal polyphosphate biosynthetic enzyme in many bacteria [20,21] using ATP as the preferred phosphate donor. Sequence similarity identified a subclass of polyphosphate kinases which shows a preference towards pyrimidine nts [22]. Examples of polyphosphate kinase 2 (PPK2) have been characterized from a wide range of bacteria [18,23–26], where the kinetics favour polyphosphate-driven ATP synthesis. The 3D-fold of PPK2 (PDB codes 3CZP, 3CZQ and 3RHF) [23] is structurally distinct from PPK1 (PDB codes 1XDP and 1XDO) [27] and belongs to a larger family of P-loop kinases [28] that feature two conserved motifs that co-ordinate the nucleoside triphosphate and Mg^{2+}, Walker A (GXXXXGK) and Walker B [23]. The Walker B motif was originally identified as hhhhD, where h represents a hydrophobic residue [29] and the aspartic acid is proposed to co-ordinate a magnesium ion. Earlier, the same aspartate in a DRS tripeptide conserved within the PPK2 family has also been termed the Walker B motif (Figure 1) [23]. The hydrolytic degradation of polyphosphate is catalysed by polyphosphatase (Ppx), resulting in the release of P_i. As part of a regulatory network, Ppx is inhibited by (p)ppGpp which increases during the stringent response [8,14], resulting in the accumulation of higher levels of polyphosphate.

Francisella tularensis is an intracellular pathogen and the causative agent of the zoonotic disease tularemia [30]. It is noted for a low infectious dose, ease of dissemination and ability to cause severe disease [31]. These properties and the associated potential as a bio-threat led to the classification of *F. tularensis* as category A (the highest priority for prevention) by the Centers for Disease Control and Prevention (CDC) [32]. The availability of genome sequence data and development of molecular tools has allowed us to start to understand the molecular basis of *F. tularensis* pathogenicity. Bacteria may have one or more polyphosphate kinase homologues within their genomes [8] and some

encode multiple polyphosphate kinase genes [23]. In *F. tularensis* subspecies *tularensis* SCHU S4, the gene FTT1564 and the homologue in *Francisella novicida,* FTN1472, were identified as encoding polyphosphate kinases of the PPK2 family (Figure 1). Inactivation of FTN1472 resulted in abolition of polyphosphate production, confirming the observation from bioinformatics analysis that this is the only polyphosphate kinase present in these strains [17].

Herein, we describe the biochemical characterization of the *F. tularensis* PPK2 encoded by FTT1564 (*Ft*PPK2), including activity assays using HPLC detection and ^{31}P-NMR to measure product formation. These assays permitted the determination of the substrate preference and kinetic parameters of *Ft*PPK2. We report the affinity of *Ft*PPK2 for polyphosphate measured by isothermal titration calorimetry (ITC). We also report the crystal structure of *Ft*PPK2 and compare it with other enzymes of the P-loop phosphotransferase superfamily, identifying the conserved structural features and probable substrate-binding sites. In addition, we report the antibiotic sensitivity of the ΔFTT1564 strain. Taken together, these studies are an important prerequisite to investigating the development of *Ft*PPK2 inhibitors as potential anti-microbials.

MATERIALS AND METHODS

Materials

NMPs, NDPs, NTPs and DMHA were purchased from Sigma–Aldrich; DTT, BSA and antibiotics were purchased from Melford Laboratories; polyacrylamide/bis polyacrylamide (30% w/v, 37.5:1) and Bacto agar were purchased from Fisher Scientific; Bacto tryptone and yeast extract for culture media were purchased from Oxoid; Chelating Fast Flow resins were purchased from GE Healthcare; primers were purchased from Eurofins; BIO-X-ACT was purchased from Bioline; restriction enzymes and *Escherichia coli* strain K12 JM109 were purchased from New England Biolabs; *E. coli* BL21 Rosetta pLysS (DE3), the pET16b plasmid and polyphosphate averaging 25 units in length was purchased from Merck Chemicals. *E coli* strain TOP10 was purchased from Invitrogen. Screens (96-well), crystal trays and coverslips were purchased from Molecular Dimensions. Unless otherwise stated, other chemicals and reagents were and purchased from Sigma–Aldrich or Fisher Scientific.

Protein expression and purification

The gene encoding *Ft*PPK2, FTT1564, was amplified from *F. tularensis* subspecies *tularensis* SCHU S4 genomic DNA using a forward primer (5′-gcggacatgttgcatcatcatcatcatcataaagttttaagtcaagaagagcgc) paired with a reverse primer (5′-cgcctcgagttatttatatattttgaagaagtgcctacgat). The PCR product was digested with PciI and XhoI and ligated into the NcoI/XhoI restricted pET16b. The resultant plasmid, pET16b/ppk, was verified by sequencing. The plasmid was chemically transformed into BL21 Rosetta pLysS (DE3). Single colonies were used to inoculate 2YT medium (10 ml containing 100 μg/ml ampicillin) and cultured overnight at 27 °C. The overnight culture was used as a 1% inoculum into flasks of 2YT medium (500 ml) which was induced with IPTG (final concentration 0.4 mM) when the D_{600} reached 0.6 and then cultured overnight at 27 °C. Cells were harvested by centrifugation (11,300 g for 20 min) and the cell pellet (typically ∼7 g/l of culture) was stored at –80 °C. To purify *Ft*PPK2, the frozen cell pellet (∼35 g) was resuspended in cold lysis buffer (3 × w/v cell pellet) and a Roche protease inhibitor tablet added. Lysozyme (5–15 mg) was added and the cell suspension was stirred (4 °C, 30 min), then sonicated on ice (4 °C, 20 × 10 s with 10-s rest). The lysate was cleared by centrifugation (Sorval evolution, SLA-1500 rotor, 4 °C, 29 752 ***g***, 30 min) and the resulting supernatant was applied (4 ml·min^{-1}) to a Ni-NTA Sepharose Fast Flow column (50 ml bed volume). The column was washed (4 ml·min^{-1}) with low imidazole buffer (∼5 column volumes, 50 mM Tris/HCl, 0.5 M NaCl, 50 mM imidazole, 20% glycerol, pH 8.0). The *Ft*PPK2 was eluted with a gradient of 0%–100% high imidazole buffer (4 column volumes, 50 mM Tris/HCl; 0.5 M NaCl; 500 mM imidazole; 20% glycerol, pH 8.0). Fractions containing *Ft*PPK2 were pooled, dialysed (2 × 1 l, 50 mM Tris/HCl; 0.3 M NaCl; 20% glycerol; 5 mM DTT, pH 8.0) and stored at –80 °C. For crystallization screening, *Ft*PPK2 was concentrated to 15 mg/ml in an Amicon pressure cell and applied to a S75 Sepharose gel filtration column (bed volume 200 ml, flow rate 2 ml·min^{-1}). The eluted *Ft*PPK2 was eluted (2 ml·min^{-1}; 50 mM Tris/HCl, 0.3 M NaCl, 20% glycerol, 5 mM DTT, pH 8) and fractions judged to be pure by SDS/PAGE analysis were pooled, concentrated to 15 mg/ml and stored as aliquots (100 μl) at –80 °C.

Ion-pair HPLC of *Ft*PPK2 activity assays

Substrate specificity of *Ft*PPK2 was analysed using an ion-pairing HPLC-based method. Reaction mixtures (1 ml) contained 50 mM Tris/HCl (pH 8.0), 0.3 M NaCl, 20% glycerol, 10 mM $MgCl_2$ and 80 mM $(NH_4)_2SO_4$, 100 μM polyphosphate (as polymer), 0–2 mM nt and were initiated by the addition of *Ft*PPK2 (250 nM). Reactions were incubated at 37 °C and at selected time points, aliquots (100 μl) were withdrawn and the reaction quenched by heating (95 °C, 5 min). Precipitated protein was removed by centrifugation (13,200 g, 5 min) and a sample (40 μl) was analysed by ion pairing HPLC [Gemini C18 column (150 × 4.6 mm 5 micron)] with detection at 260 nm using the following solvents: organic, 80% methanol, 15 mM DMHA, pH 7.0, aqueous; 5% methanol, 15 mM DMHA, pH 7.0. The solvents were adjusted to pH 7.0 with acetic acid. The column was equilibrated in 25% organic at a flow rate of 0.8 ml·min$^{-1.}$ After sample injection, the following elution profile was applied: 5 min isocratic (25% organic) and then a 22 minute linear gradient to 55% organic, followed by a 5 minutes isocratic at 55% organic, 5 min gradient to 25% organic and 5 min isocratic at 25% organic. Absorbance measurements were converted into concentrations of NTPs and NDPs using calibration curves and plotted as reaction time courses. For competition assays, the formation of

product nts were empirically fitted to a single exponential rise to a maximum, $[P] = [P]_{max}(1 - e^{-kt})$. Using the rate constant k, the initial rate of product formation, v, was calculated ($v = k[P]_{max}$). For steady state kinetics, the time course of product formation was fitted to a linear function to give the initial rates which were then fitted to a classical Michaelis–Menten kinetic model.

Metal ion and pH dependence of *Ft*PPK2

Substrate specificity of *Ft*PPK2 was analysed using an ion-pairing HPLC-based method. Reaction mixtures (500 μl) contained 50 mM Tris/HCl (pH 8.0), 0.3 M NaCl, 20 % glycerol and 80 mM $(NH_4)_2SO_4$, 30 μM polyphosphate, 0.2 mM ADP and were initiated by the addition of *Ft*PPK2 (30 nM). $MnCl_2$ and $MgCl_2$ concentrations from 0.25 to 50 mM and a pH range from 5.5 to 9 were used, MES (50 mM) for the pH 5.5–6 and bis-tris propane (50 mM) for pH 6.5–9. Reactions were incubated at 30 °C and, after 3 min, aliquots (100 μl) were withdrawn and the reaction quenched using EDTA (50 mM), followed by heating (95 °C, 5 min). Precipitated protein was removed by centrifugation (13,200 g, 5 min) and a sample (40 μl) was analysed by ion pairing HPLC [Gemini C18 column (150 × 4.6 mm, 5 micron)] with detection at 260 nm using the same separation method described above.

Isothermal titration calorimetry

All experiments were carried out using a MicroCal VP-ITC calorimeter (MicroCal, Inc.) at 310 K, unless otherwise stated, while stirring at 500 rpm. Experiments were carried out in ITC experimental buffer (50 mM HEPES, pH 8.0, 10 mM $MgCl_2$, 0.3 M NaCl, 20 % glycerol, 0.15 mM β-mercaptoethanol). *Ft*PPK2 was exchanged into this buffer by dialysis and size exclusion including chromatography. Titrations began with an initial injection of 2 μl followed by 39 identical injections of 5 μl. Data were corrected for heats of dilution by subtracting the data from independent titrations of ligand into buffer. Data were fitted to a bimolecular binding model using MicroCal™ Origin software. Experiments were carried out in duplicate.

^{31}P-NMR *Ft*PPK2 activity assays

The overall reaction time course of an *Ft*PPK2 catalysed reaction was monitored with ^{31}P-NMR. Using standards of ADP and polyphosphate, the relaxation time (T_1) was optimized to ensure integrals derived from spectra accurately reflected the concentrations of all ^{31}P species in the reaction mixture. The signal from nt dCMP (2 mM) was used as an internal standard. The assay mixture (2.5 ml) contained 50 mM Tris/HCl, pH 8.0, 0.3 M NaCl, 20 % glycerol, 10 mM $MgCl_2$, 80 mM $(NH_4)_2SO_4$, 10 % ^2H_2O, 500 μM polyphosphate and up to 2 mM nt substrate. The reaction was initiated through the addition of 150 nM *Ft*PPK2, mixed and data collected at 37 °C for 543 s followed by 453-s bins for the duration of the assay. Peak integrals were converted into concentrations using the dCMP standard as a calibrant and the concentration data used to plot time courses, which were fitted to an empirically selected function, either a first order or a linear process.

*Ft*PPK2 crystallization and structure determination

Initial crystallization conditions were identified using the Hampton Research crystal screen 1 using the sitting drop vapour diffusion method. Conditions for crystallization of *Ft*PPK2 were optimized in 24-well format by the hanging drop vapour diffusion method at 20 °C. For X-ray data collection, *Ft*PPK2 was crystallized using a precipitant solution containing: 0.8 M Na citrate, 0.1 M Na HEPES (pH 8.5), 2.5 mM AMP–PNP and 1 mM $MgCl_2$. Diffraction data were collected on the i02 beamline at the Diamond Light Source. The data were processed with xia2 [33] and the structure was solved by molecular replacement with the BALBES software [34], which also incorporates the Arp/Warp software [35]. The model was built with COOT [36] and refined with Phenix refine [37]. The data collection and refinement statistics are shown in Table 2.

Antibiotic sensitivity testing of the ΔFTT1564 *F. tularensis* mutant

All work with *Francisella* strains was performed in a containment level III laboratory in accordance with relevant legislative requirements The *F. tularensis* SCHU S4ΔFTT1564::CAM mutant [17] was tested for susceptibility to various classes of antibiotics. *F. tularensis* SCHU S4 and the ΔFTT1564 mutant strain, were inoculated from a fresh blood cysteine glucose agar (BCGA) plate into 25 ml of brain heart infusion broth to D_{600} of 0.1, then the cultures were incubated overnight with shaking at 37 °C. Cultures were adjusted to a D_{600} of 1.0 with fresh culture medium. In three biological replicates, aliquots of 1 ml of *F. tularensis* SCHU S4 or the ΔFTT1564 mutant were pipetted on to dry BCGA plates and surplus media removed. Sterile discs (BBL™ Sensi-Disc™ Susceptibility Test Discs) 5 mm in diameter, impregnated with an antibiotic, were placed in triplicate on the plate using sterile forceps. The total quantities of antibiotic on each disc were: streptomycin, 10 μg; gentamycin, 10 μg; tetracycline, 30 μ; doxycycline, 30 μg; ciprofloxacin, 5 μg and polymyxin B, 100 μg. The plates were incubated face-up, for 24 h at 37 °C and zones of inhibition in the lawns surrounding the discs measured. The mean results from three independent experiments, conducted in technical triplicates were analysed using an unpaired *t*test with Welch's correction for unequal variance using GraphPad Prism V6.02.

RESULTS

Expression and purification of *Ft*PPK2

Heterologous expression *Ft*PPK2 in *E. coli* was greatly improved by using the BL21 Rosetta pLysS (DE3) strain to overcome

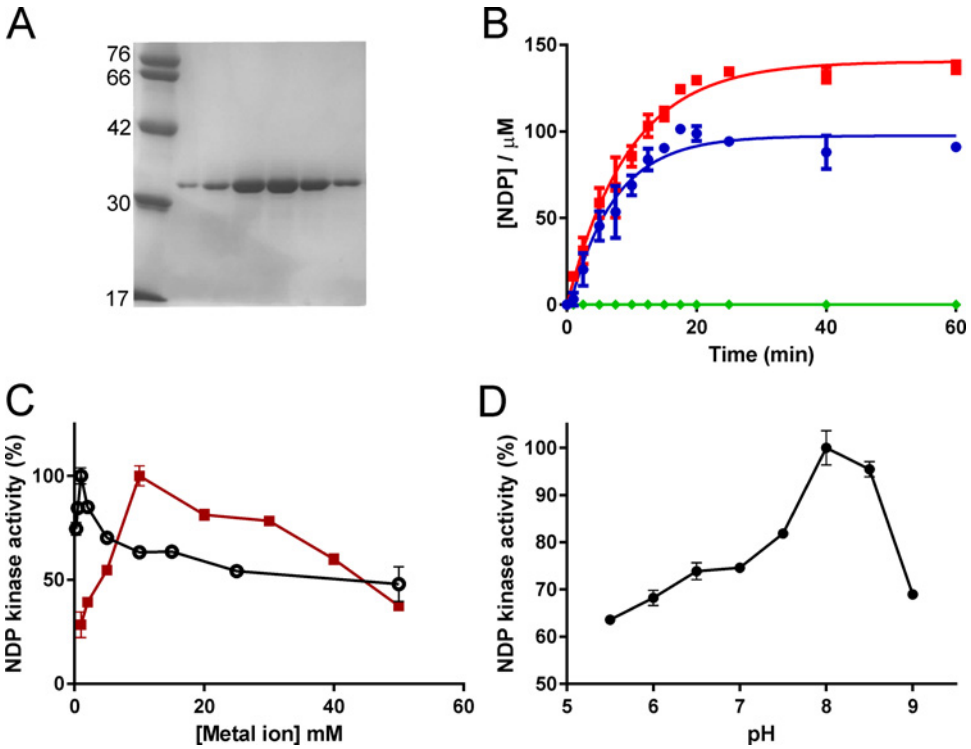

Figure 2 **Characterization of *Ft*PPK2**

(**A**) SDS/PAGE analysis of fractions from the final purification step (Superdex 75 size exclusion chromatography). (**B**) Formation of NTPs in *Ft*PPK2 activity assays. Concentrations of NTPs were measured by IP–HPLC. Red squares: ATP; blue circles: GTP; green diamonds: UTP. Reagents were added at the following initial conditions: polyphosphate: 0.1 mM; *Ft*PPK2: 250 nM; NDPs: 500 μM; 37 °C. (**C**) Metal ion dependence of *Ft*PPK2. Black open circles: Mg^{2+}; red squares: Mn^{2+}. (**D**) pH dependence of *Ft*PPK2. Activity in (**C**) and (**D**) has been normalized to the maximum (100 %).

the problem of codon bias and the A + T rich nature of the *F. tularensis* sequence (66 %). Affinity purification with the incorporated His_6-tag yielded 6 mg of purified *Ft*PPK2/g cell paste and *Ft*PPK2 was stable (over 3 months) when stored as aliquots in buffer containing 20 % glycerol at –80 °C. Further purification by size exclusion chromatography (Superdex 75) yielded highly purified *Ft*PPK2 suitable for protein crystallization studies (Figure 2A).

Substrate specificity of *Ft*PPK2

To investigate the substrate preference of *Ft*PPK2, competition activity assays were prepared containing pairs of nucleoside diphosphate analogues (ADP and GDP; ADP and CDP; ADP and UDP) and analysed for formation of the triphosphate product by ion pairing HPLC (Figure 2B). The initial rate was 0.250 ± 0.052 μmol/s for formation of ATP as product and 0.244 ± 0.026 μmol/s for formation of GTP, but UDP and CDP were not substrates under these conditions. Single time point activity assays (quenched at 60 min) were prepared with AMP and GMP (500 μM) as substrates. No formation of nt diphosphates was detected, which demonstrated that AMP and GMP were not substrates for *Ft*PPK2 (result not shown).

Metal ion and pH dependence of *Ft*PPK2

The optimal concentrations for divalent cations Mg^{2+} and Mn^{2+} with *Ft*PPK2 were 10 and 1 mM respectively (Figure 2C). A lower optimal concentration for Mn^{2+} ions than Mg^{2+} ions has been observed for other PPK2 enzymes [18,23]. *Ft*PPK2 was active over a wide range of pH values, with optimal activity at pH 8 (Figure 2D). The sharp drop-off in activity at pH 9 may have resulted from deprotonation of either a catalytic residue or a protonated basic residue that acts as a counter ion to the polyphosphate and nt substrates.

Nt substrate steady state kinetics

As shown in the previous section, *Ft*PPK2 uses both GDP and ADP as substrates and the data indicated that both these substrates were used with approximately equal efficiency. The IP–HPLC assay was then used to quantify (in duplicate) the rates of formation of reaction products in *Ft*PPK2 catalysed reactions, in both

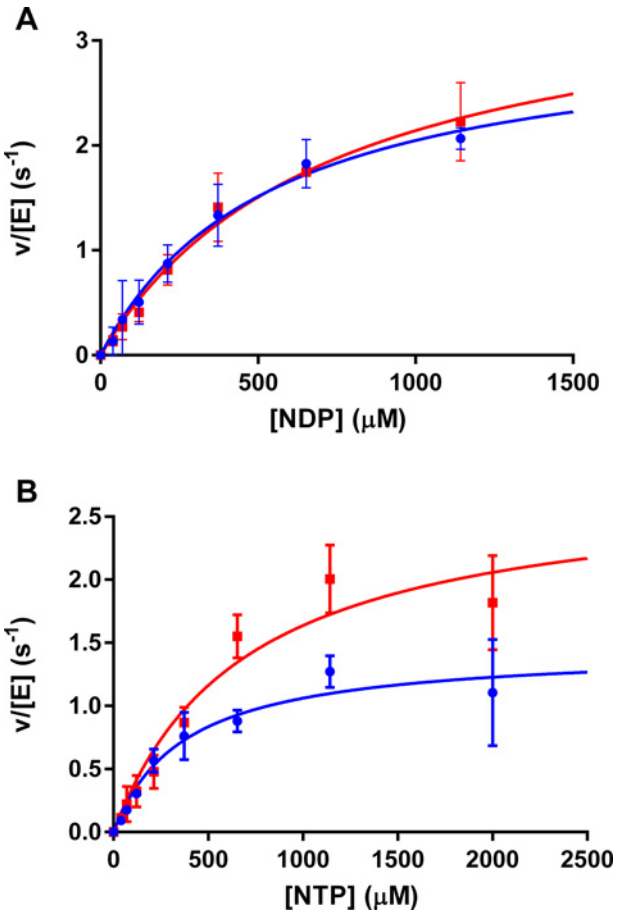

Figure 3 Steady state kinetic analysis of *Ft*PPK2 substrate specificity

(**A**) Nucleoside diphosphate substrates, (**B**) nucleoside triphosphate substrates. Adenosine nts: blue circles; guanosine nts: red squares. Reagents were added at the following concentrations: polyphosphate: 0.1 mM; *Ft*PPK2: 150 nM. Goodness of fit (R^2) for each nt was: GDP: 0.99; ADP: 0.99; GTP: 0.95; ATP: 0.97.

directions. For the triphosphate forming reaction, GDP and ADP were used as substrates and the formation of GTP and ATP products were measured. For the reaction in the reverse direction (forming diphosphates), GTP and ATP were used as substrates and the formation of GDP and ADP products were measured. Measurements were made with substrate nts (GDP, ADP, GTP and ATP) concentrations over a range 0–2 mM at 37 °C. Fitting the derived initial rates to Michalis–Menten steady state kinetics (Figure 3) gave the k_{cat} and K_M parameters for *Ft*PPK2 which are compared with values for other members of the PPK2 family [23] in Table 1. In the activity assays with nucleoside triphosphates as substrates (Figure 3B), a fine precipitate was occasionally observed to form in assays at higher NTP concentrations (>500 μM). This may account for the observed larger error bars for these activity measurements. The calculated catalytic efficiency (k_{cat}/K_M) is broadly similar for guanine and adenine nts and for bis- or triphosphate substrates.

Table 1 Steady state kinetic parameters for *Ft*PPK2 from activity measurements using IP–HPLC. *Data for *S. meliloti* PPK2 (SMc02148) from Nocek et al.[23].

Substrate	Measured product	k_{cat}/s^{-1}	$K_M/\mu M$	$k_{cat}/K_M/s^{-1}.M^{-1}$
ADP	ATP	3.17 ± 0.22	546 ± 79.2	5788 ± 1242
ATP	ADP	1.46 ± 0.13	372 ± 90.5	3920 ± 1301
GDP	GTP	3.69 ± 0.37	727 ± 138	5075 ± 1472
GTP	GDP	2.77 ± 0.41	692 ± 235	4002 ± 1951
*ADP		7.60 ± 0.01	32.0 ± 4.10	23800
*GDP		0.80 ± 0.03	520 ± 70.0	1538

Substrate binding to *Ft*PPK2 by isothermal titration calorimetry

To measure the binding affinity of substrates to *Ft*PPK2, we used ITC. The results of these titration experiments (Figure 4) showed no discernible substrate binding for a nt substrate in the absence of polyphosphate, but titration of polyphosphate in the absence of nts fitted to a single binding site model ($N = 0.63 \pm 0.01$) with the following thermodynamic parameters: $K_a = 8.21 \pm 3.29 \times 10^6$, $\Delta H = -6.09 \pm 0.17$ kcal/mol (1 kcal ≡ 4184 J) and $\Delta S = 11.2$, equivalent to a K_d of 122 nM. This data suggest that significant binding of the nt substrate requires the presence of polyphosphate.

^{31}P-NMR *Ft*PPK2 activity assay

The overall reaction time course of an *Ft*PPK2 catalysed reaction was monitored with ^{31}P-NMR (Figure 5). Using standards of ADP and polyphosphate, the relaxation time (T_1) was optimized to ensure integrals derived from spectra accurately reflected the concentrations of all ^{31}P species in the reaction mixture. The signal from nt dCMP (2 mM) was well separated from any substrate- or product-derived signals and was used as an internal standard (Figure 5A, green). The assay mixture (2.5 ml) contained 50 mM Tris/HCl (pH 8.0), 0.3 M NaCl, 20% glycerol, 10 mM $MgCl_2$, 80 mM $(NH_4)_2SO_4$, 10% ^2H_2O, up to 500 μM polyphosphate and up to 2 mM nt substrate. The reactions were initiated through the addition of 150 nM *Ft*PPK2, mixed and data collected at 37 °C for 543 s followed by 453-s bins for the duration of the assay. Qualitatively, the time-dependent utilization of the ADP [signals at –5.94 (β-ADP) and –10.07 (α-ADP) ppm] and the internal phospho-anhydrides of polyphosphate (–23.39 ppm) can be observed, as can the corresponding formation of ATP [signals at –5.44 (γ-ATP) –10.72 (α-ATP); –18.96 (β-ATP) ppm]. No signal for the formation of P_i or other phosphorus containing by-product appeared, suggesting the *Ft*PPK2 catalysed phosphotransfer reaction is efficient, without any significant competing hydrolytic or other side reaction. Using the dCMP standard as an internal calibrant, the integrals were converted into concentrations for each time point. Plotting these concentrations against time gave a reaction time course for ATP, ADP (Figure 5B) and polyphosphate internal phosphoanhydride (Figure 5C). Comparing time courses initiated at high and low polyphosphate concentrations (500 and 16 μM respectively) reveals the limitation of this experimental

Table 2 Rate constants from ^{31}P-NMR time courses of *Ft*PPK2 assays

Experiment*	Initial [PolyP] / μM	Kinetic parameters†	Nts	
			ATP	ADP
1	500	$k_1 \times 10^{-3}/s^{-1}$	1.52 ± 0.17	1.02 ± 0.14
		R^2	0.99	0.99
		$\Delta C/\mu M$	1750 ± 73	1880 ± 36
		Initial rate/$\mu M \cdot s^{-1}$	2.65 ± 0.41	1.915 ± 0.30
2	16	$k_1 \times 10^{-3}/ s^{-1}$	0.769	ND‡
		R^2	0.98	ND
		$\Delta C/\mu M$	556	ND
		Initial rate/$\mu M \cdot s^{-1}$	0.450	ND

*Reactions also contained 150 nM *Ft*PPK2, 2 mM nt, 2 mM CMP (internal standard) and 10% v/v ^2H_2O.
†Time courses were fitted to a first order process: k_1, first order rate constant; R^2, goodness of fit; ΔC, calculated change in concentration of nt.
‡ND, not determined (a reliable fit could not be achieved).

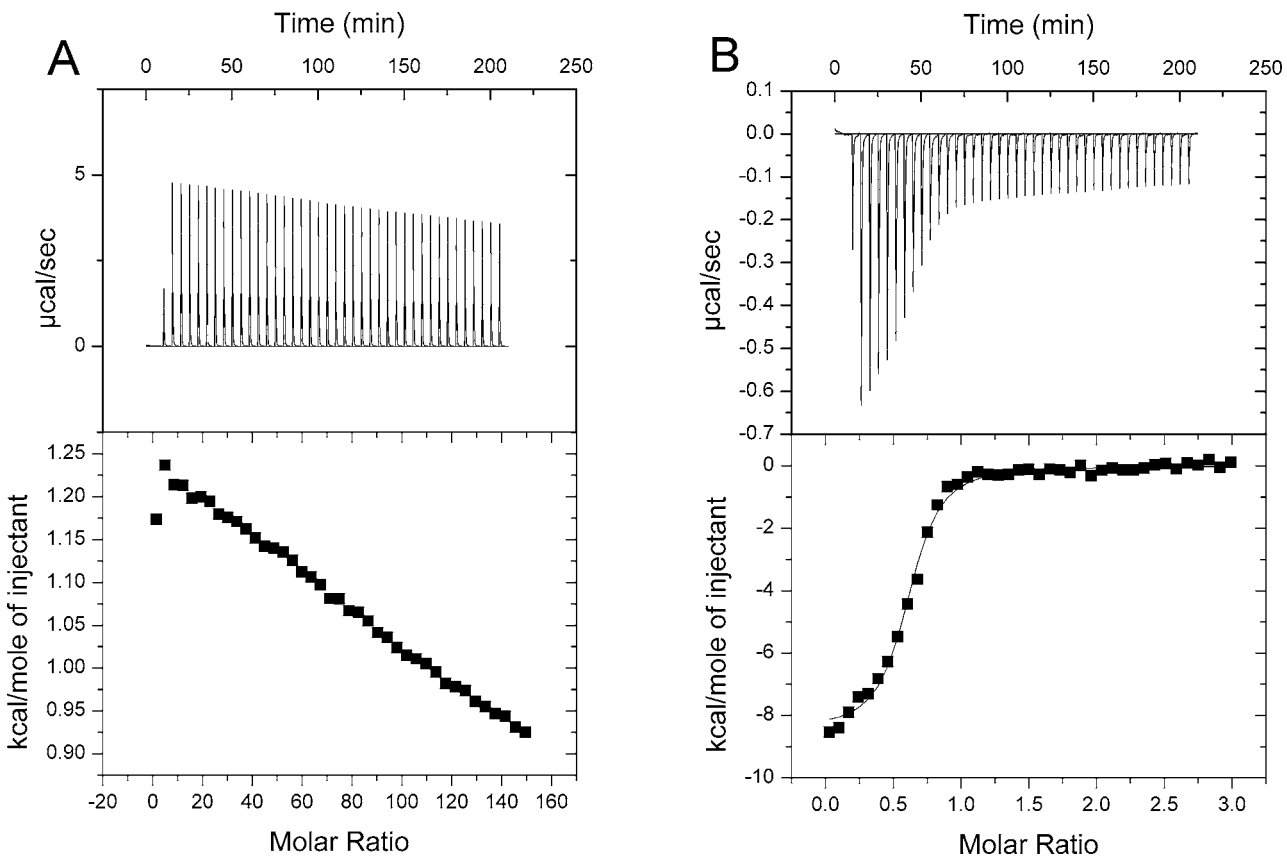

Figure 4 ITC analysis of *Ft*PPK2 substrate binding
(**A**) Titration of ADP into *Ft*PPK2. (**B**) Titration of polyphosphate into *Ft*PPK2. Titration conditions: 50 mM HEPES (pH 8), 10 mM $MgCl_2$, 0.3 M NaCl, 20% (v/v) glycerol, 0.15 mM β-mercaptoethanol, 298 K.

approach, as the errors in the integrals at lower polyphosphate concentrations become too large. For example, using 500 μM polyphosphate (Table 2, experiment 1), the kinetic parameters for fitting the time courses of ATP formation and ADP depletion approximately match, as does the total change in concentrations and the calculated initial rates. However, the results at 16 μM polyphosphate, while qualitatively heading in the expected direction, cannot be fitted to give well correlated results. A similar caveat must be placed on integrals of the internal phosphate signal of polyphosphate, which both qualitatively show a decrease

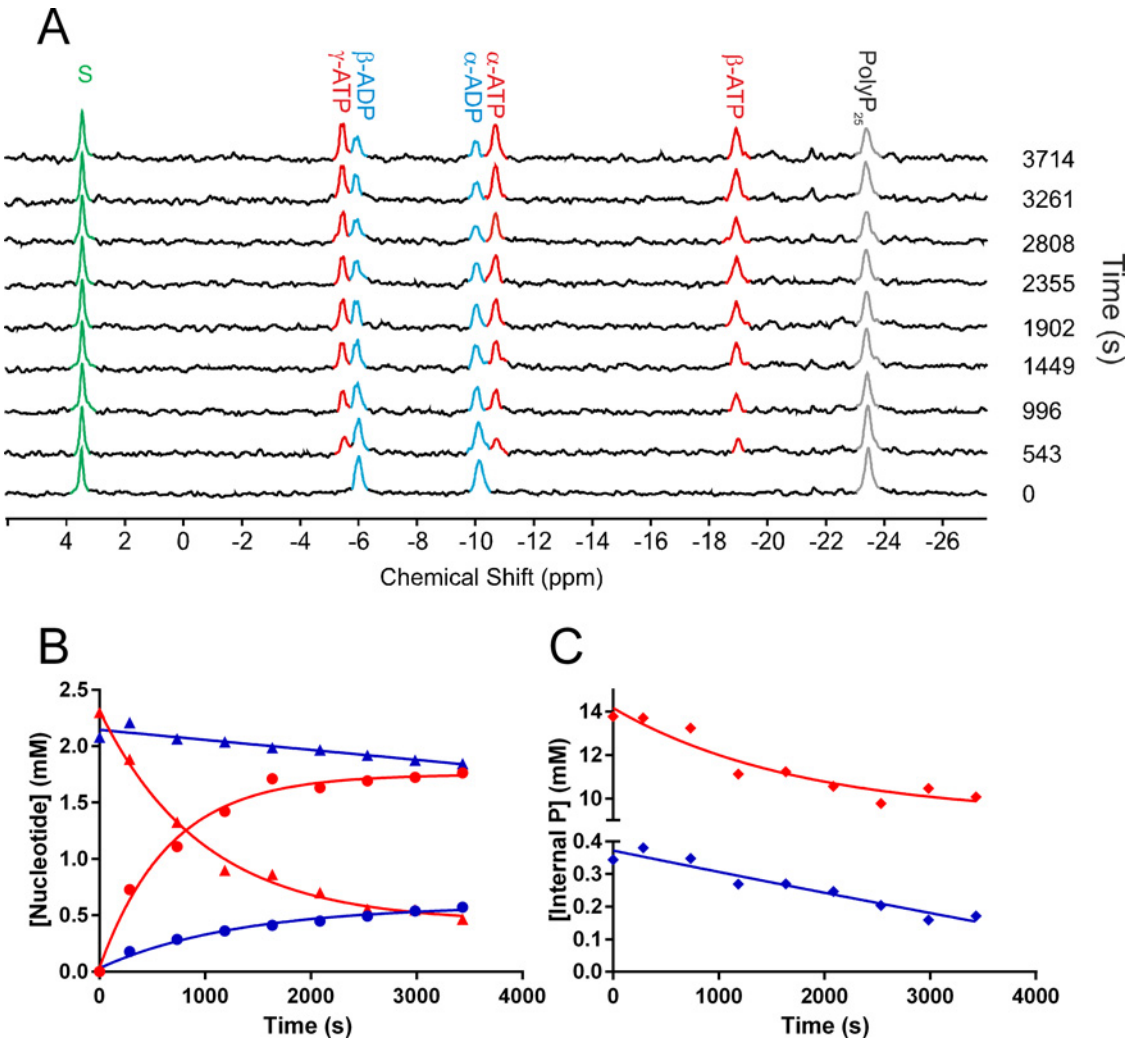

Figure 5 Kinetic analysis of *Ft*PPK2 catalysed reactions using ^{31}P-NMR

(**A**) Time course for a *Ft*PPK2 reaction monitored by ^{31}P-NMR. In this example reaction, initial conditions were: 2 mM ADP, 125 μM polyphosphate, 2 mM dCMP and 150 nM *Ft*PPK2. Peaks were assigned as follows: 3.44 (dCMP), –5.44 (γ-ATP), –5.94 (β-ADP), –10.07 (α-ADP), –10.72 (α-ATP), –18.96 (β-ATP), –23.39 (polyphosphate internal phosphoanhydride); peaks are coloured as follows: ATP: red; ADP: blue; polyphosphate internal phosphoanhydride: grey; dCMP: green. (**B**) Kinetics analysis of ^{31}P-NMR time course experiments for two nt concentrations. Experiment 1 (initial [polyphosphate] = 500 μM); ATP: red circles, ADP: red triangles. Experiment 2 (initial [polyphosphate] = 16 μM); ATP: blue circles, ADP: blue triangles. (**C**) Kinetic analysis of ^{31}P-NMR time course experiments for changes in internal phosphoanhydride in polyphosphate. Red: experiment 1; blue: experiment 2. The spectrometer (Bruker 400 MHz, operating at 161 MHz for ^{31}P-NMR) was maintained at 37 °C for the duration of the experiment.

but the small change in a relatively large integral could not be reliably fitted (Figure 5C).

X-ray crystal structure of *Ft*PPK2

Screening using the sitting drop vapour diffusion method yielded *Ft*PPK2 crystals with a sodium citrate precipitant and HEPES buffer (pH 8.4) in the presence of the non-hydrolysable ATP analogue adenylyl imidodiphosphate (AMP–PNP) [38]. The crystals formed overnight and reached a maximum size after 3 days. Conditions were optimized to produce crystals up to 200 μm in the longest dimension which diffracted to a 2.23 Å (1 Å = 0.1 nm) resolution at Diamond beamline i02 (Table 3). The *Ft*PPK2 structure was solved by molecular replacement using the *Sinorhizobium meliloti* PPK2 structure (SMc02148, PDB ID: 3CZQ) as a model and the BALBES pipeline [34]. The refined structure of *Ft*PPK2 reveals four monomers in the asymmetric unit in a D2 tetrameric organization (Figure 6A). Despite the inclusion of AMP–PNP in the crystallization solution, no density corresponding to this ligand was observed. Each monomer consists of a six-strand β-sheet, surrounded by 10 α-helices, with the insertion of a lid motif (helices 8 and 9; Figures 6B and 6C).

Table 3 Crystallographic data for *Ft*PPK2.
Figures in brackets indicate the highest resolution shell.

Data Set	*Ft*PPK08
Resolution of data (outer shell; Å)	81.65–2.23 (2.27–2.23)
Space group	$P2_12_12_1$
Unit cell parameters	a = 86.79, b = 88.89, c = 163.3 a = b = c = 90°
R_{merge} (overall, all I+ and I–)	0.052 (0.539)
Mean I/σI (outer shell)	15.5 (2.4)
Completeness (outer shell; %)	99.2 (99.7)
Multiplicity (outer shell)	3.6 (3.5)
No. unique reflections	61793
R_{work}	0.20
R_{free}	0.25
Number protein atoms	8412
Number solvent waters	473
Number ligand atoms	None
RMSD for bonds (Å)	0.009
RMSD for angles (°)	1.220
Average protein B factor	31.6
Average lid module B factor	45.8
Average solvent B factor	48.8
PDB entry	4YEG

Table 4 Dali analysis for FtPPK2.
Results for the five structures that are most similar to *Ft*PPK2 are shown.

Model PDB code	Average Z-score	Average RMSD (Å)	Sequence Identity (%)
3CZQ	31.78	1.73	47.0
3CZP	24.65	2.25	33.0
3RHF	24.75	2.53	26.8
4NZY	11.65	3.2	29.5
2PLR	11.6	3.25	18.5

A Dali search [39] for structural similarity identified PPK2 from *S. meliloti* as the closest related protein structure, followed by the PPK2 protein from *Pseudomonas aeruginosa* (PA3455, PDB ID: 3CZP) [23] and *Arthrobacter aurescens* (AAur_2811, PDB ID: 3RHF). The next most similar structures are two thymidylate kinases, from *Sulfolobus tokodaii* STK_15430, PDB ID: 2PLR) and *Staphylococcus aureus* (SAV0482, PDB ID: 4EAQ) respectively (Table 4).

Comparison of *Ft*PPK2 and *S. meliloti* PPK2 (Figure 7A) shows high structural similarity in most areas (RMSD 0.782 Å for all atoms), apart from the N-terminus, Walker A motif and lid module. Like the *S. meliloti* structure, *Ft*PPK2 has a central six-stranded parallel β-sheet flanked by α-helices at the side and top. The lid module of *Ft*PPK2 is not covered by the N-terminal extension domain present in the *S. meliloti* structure and the *Ft*PPK2 lid module appears to be in a slightly more open conformation (Figure 7B). Parts of the electron density for the lid module for fully refined *Ft*PPK2 cannot be resolved for chains C (missing residues 181–192) and D chains (missing residues 182–188), which may point to a high degree of flexibility in this region. This flexibility may also be reflected in the lid B factors which are higher in the lid motif (for example, residues 168–198, chain A, mean B = 45.8 Å^2) than the mean for the whole structure (all residues, chain A, mean B = 31.6 Å^2; Figure 7C).

Nocek et al. [23] postulated that the nt substrate binds to PPK2 to one side of the Walker A-motif containing loop, which in *Ft*PPK2 corresponds approximately to the area between Asp^{117} and Phe^{132}, forming a pocket between α helices 6 and 7 (Figures 6 and 8A). They suggested that a conserved aspartic acid residue (corresponding to *Ft*PPK2 Asp^{117}; Figure 8A) in the Walker B motif may co-ordinate a magnesium ion required for substrate binding and potentially for catalysis. In addition they identified a conserved lysine residue in the Walker A motif (corresponding to *Ft*PPK2 Lys^{66}; Figure 8A) which they anticipated may bind the β- and γ-phosphates of ATP in the active site.

*Ft*PPK2 has a large positively charged region (on the left hand side of the Walker A motif as shown in Figure 8B), made up of residues His^{76}, Arg^{174}, Lys^{228}, Lys^{229} and Arg^{232}. We propose these residues constitute the polyP substrate-binding pocket, which is sufficiently long (18 Å) to accommodate approximately eight residues of the polyphosphate chain (calculated maximum length 21 Å). Using this arrangement, the terminal phosphate of the polyP and the nt are correctly juxtaposed below the lid, in the region of the Walker A motif and the catalytically important Lys^{66} and Asp^{62}. Higher B-factors indicate that the Walker A motif is a flexible region and the N-terminal region of helix 3, around Asp^{62} in the *Ft*PPK2 structure, adopts a different conformation to the *S. meliloti* PPK2 structure, with some atoms moving as much as 5.9 Å (Figure 7B), although the functional significance of this movement is difficult to ascertain without precise knowledge of the substrate-binding modes. There are several conserved basic residues in the lid module that are close enough to interact with the poylphosphate ligand: Arg^{178}, Arg^{174} and Lys^{184}. The two arginine residues, Arg^{174} and Arg^{178}, form part of a motif (R-X_{2-3}-R) conserved in the lid of bacterial PPK2s [40]. The conserved Arg^{118} of the Walker B motif is anticipated to potentially form hydrogen bonds with the β- and γ-phosphates of the nt substrate.

Antibiotic sensitivity of *F. tularensis* ΔFTT1564 mutant

The effect of inactivation of polyphosphate production in *F. tularensis* on antibiotic susceptibility was determined (Figure 9). Relative to the wild-type strain, the ΔFTT1564 mutant was significantly more sensitive to killing by antibiotics targeting the translational machinery [41], namely streptomycin (10 μg, $P = 0.0048$), gentamicin (10 μg, $P = 0.0048$), tetracycline (30 μg, $P = 0.0357$) and doxycycline (30 μg, $P = 0.0028$). The ΔFTT1564 *F. tularensis* mutant was also more susceptible to killing by the topoisomerase/gyrase inhibitor ciprofloxacin, (5 μg, $P = 0.0286$). However, the mutant showed no difference in susceptibility to the membrane-targeting compound polymyxin B.

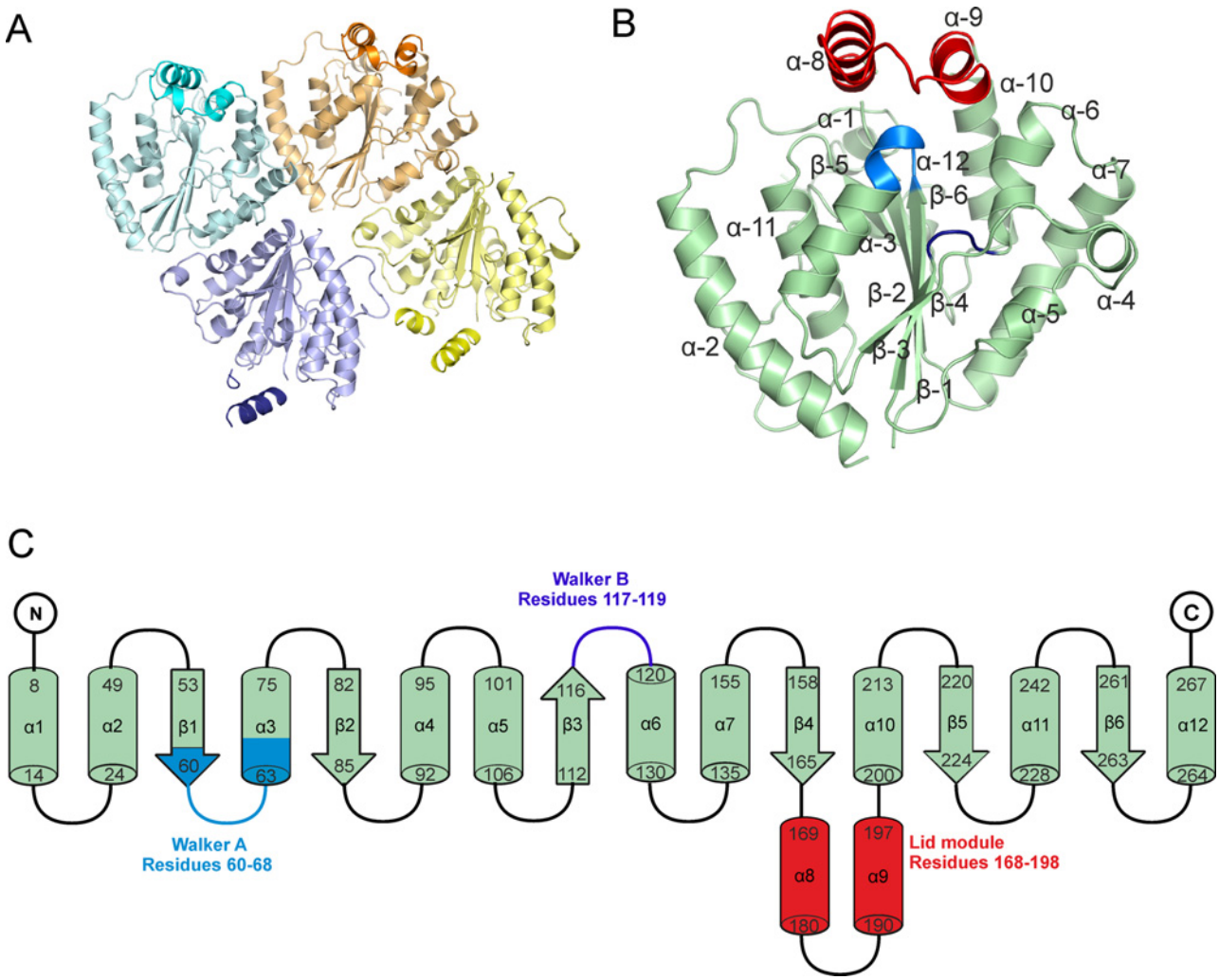

Figure 6 **Overall structure of *Ft*PPK2**

(**A**) Tetrameric organization of *Ft*PPK2 within the asymmetric unit. (**B**) *Ft*PPK2 monomer A, labelling the α-helices (α-1–12) and strands of β-sheet (β-1–6). The lid-loop motif, including helices α-8 and α-9, is coloured red, the Walker A and B motifs are coloured blue and purple respectively. (**C**) Topology diagram colour coded as in (B).

DISCUSSION

The characterization of *Ft*PPK2 through the HPLC assay format has enabled measurement of substrate preference and specificity (Figure 2; Table 1), identifying that *F. tularensis* polyphosphate kinase belongs to the PPK2 family [18,23,24,42]. *Ft*PPK2 did not accept pyrimidine nt or purine monophosphate substrates, but comparing activity with the purine substrates, it showed little substrate preference between guanosine and adenosine nts. This is comparable with the observed small preference of *M. tuberculosis* PPK2 [18] for ATP ($K_M = 330\ \mu M$) over GTP ($K_M = 660\ \mu M$), but very different from *S. meliloti* PPK2 [23] which shows a 10-fold difference in K_M, preferentially utilizing ADP over GDP (Table 2).

Sequence analysis has indicated that polyphosphate kinase enzymes are widely distributed in prokaryotes [8]. Some bacteria have a single polyphosphate kinase, either of the PPK1 or of the PPK2 subtypes and other species of bacteria contain multiple polyphosphate kinase sequences, including a mixture of subtypes [8]. Analysis of the genomes of *F. tularensis* subspecies *tularensis* SCHU S4 and subspecies *novacida* indicates that genes FTN1472 and FTT1564 respectively encode a member of the PPK2 family [17]. Moreover, biochemical evidence from the knockout mutant verified this to be the only gene encoding a polyphosphate kinase [17]. *Francisella* spp. are renowned for having compact genomes [43] and therefore there may be a competitive advantage to avoiding having multiple polyphosphate kinases when one broader specificity enzyme will do.

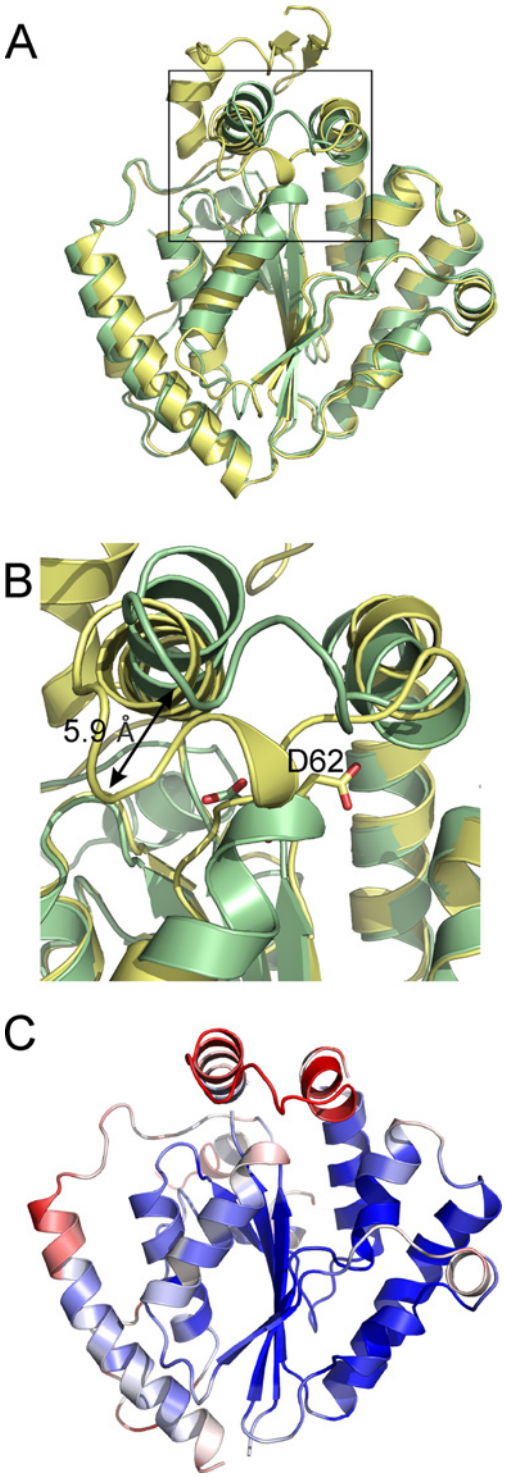

Figure 7 Similar and flexible regions of PPK2

(**A**) Overlay of the *F. tularensis* (pale green, PDB: 4YEG) and *S. meliloti* (pale yellow, PDB: 3CZQ) PPK2 structures. (**B**) Detail of the active site region [boxed region in (A)] highlighting the movement in the lid module (up to 5.9 Å) and the movement of the Walker A motif aspartic acid residue (*Ft*PPK2 D62 and *Sm*Ppk D93). (**C**) Structure of *Ft*PPK2 coloured by B-factors, ranging from blue (20 Å^2) to red (50 Å^2).

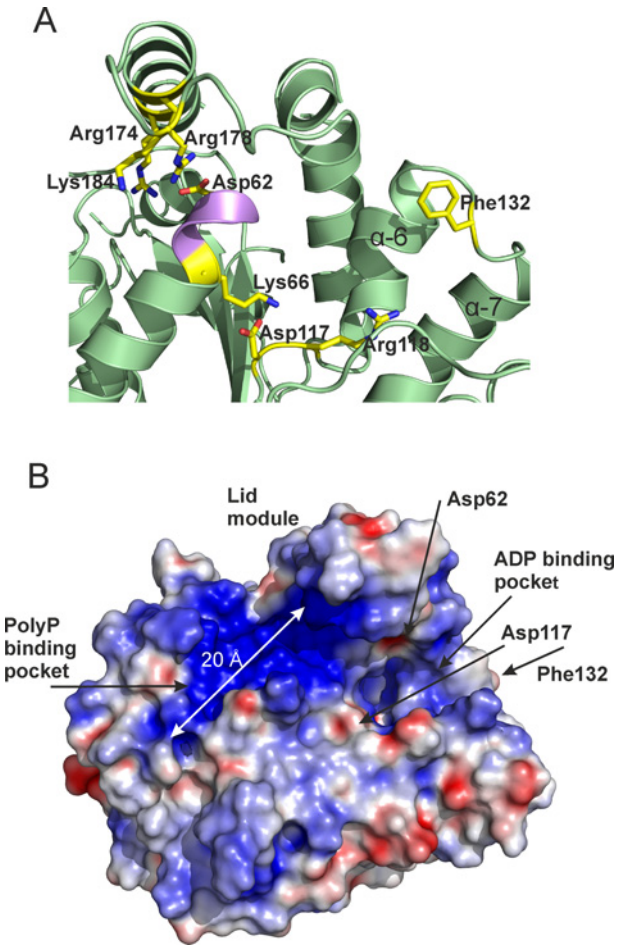

Figure 8 Active site of *Ft*PPK2

(**A**) Residues close to the active site with proposed roles in substrate binding or catalysis. (**B**) *Ft*PPK2 with an electrostatic surface, showing proposed substrate-binding sites and the location of residues with proposed roles in catalysis. Electrostatic map generated with APBS [50] using a –20 to +20 scale.

Measuring the formation of a product nt by HPLC has a significant limitation, as the sensitivity of absorbance at 260 nm limits accurate measurement of nts from assay mixtures to approximately 5 μM; below this point, the errors become unacceptable. This was not an issue for the nt substrates (K_M's in the range 300–800 μM), but the K_M for polyphosphate was significantly lower and could not be accurately measured with the HPLC-based assay. Using ITC (Figure 4), the binding of polyphosphate could be quantified for a single binding site and gave a sub-micromolar binding constant. This contrasted with the lack of nt binding observed in the absence of polyphosphate. Further characterization of *Ft*PPK2 with respect to polyphosphate turnover was achieved using ^{31}P-NMR analysis. On a qualitative basis, the ^{31}P-NMR assays confirmed the utilization of polyphosphate and ADP as substrates and the formation of ATP. The limited sensitivity of the ^{31}P-NMR restricted quantitative measurements of activity to assays containing relatively high concentrations of substrates

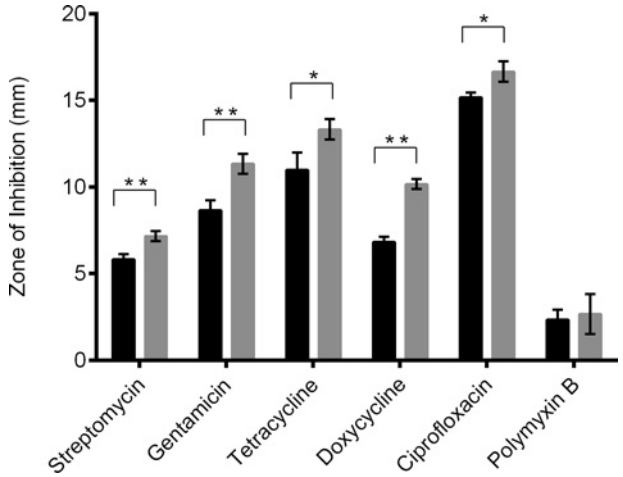

Figure 9 Antibiotic sensitivity of *F. tularensis* SCHU S4 wild-type and mutant strain ΔFTT1564

Zones of inhibition were measured in bacterial lawns surrounding antibiotic impregnated discs. Black bar: wild-type; grey bar: ΔFTT1564 mutant. Statistical significance determined by unpaired *t*test with Welch's correction for unequal variance ($*P \leqslant 0.05$, $**P \leqslant 0.01$).

(initial [NDP] = 2 mM; initial [polyphosphate] = 500 μM): under these conditions, there was a good correlation of ATP formed and ADP utilized and the associated rate constants (Table 2, initial [polyphosphate] = 500 μM). Interestingly, the fidelity of the phosphotransfer reaction proved to be excellent: over the relatively long time course of these experiments (over 1 h corresponding to more than 10000 turnovers), by-products of hydrolysis such as P_i were not observed to accumulate to a measurable extent.

There is a high degree of similarity between the structures of *Ft*PPK2 and *S. meliloti* PPK2 enzymes (Figure 7A), although the *Ft*PPK2 sequence is shorter than the other structurally characterized PPK2 enzymes and lacks the N-terminal domain present in the *P. aeruginosa* sequence (up to residue ~60 of PA0141, accession code UniProtKB Q8GCQ3) [25]**.** In terms of active site binding, ITC identified that *Ft*PPK2 does not significantly bind nt substrates in the absence of polyphosphate, which may explain the lack of observable ligand density for a nt in the structure of a crystal grown in the presence of AMP–PNP. Analysis of the surface electrostatic potential has identified an extensive positively charged region suitable for polyphosphate binding. Nocek et al. [23] proposed NDP/NTP binding between helices 6 and 7, but the molecular basis for substrate selectivity (purine compared with pyrimidine, guanosine compared with adenosine) and assignment of precise roles for active site residues during catalysis will require further experimental evidence, either from mutagenesis or from structural analysis of *Ft*PPK2 co-crystallized with substrate(s) or structural analogue(s). It seems likely that residues in the lid module are involved in substrate binding [23] and it will be interesting to determine if there is the same flexibility in the lid module in a substrate-bound *Ft*PPK2 structure or not.

As polyphosphate appears to be an important metabolite contributing to survival of *F. tularensis*, it was important to ensure that abolition of polyphosphate production did not inadvertently induce a stress response that made the pathogen more resistant to clinically relevant antibiotics. Disc diffusion experiments indicated that decreased polyphosphate production in *F. tularensis* led to increased antibiotic sensitivity to various classes of anti-microbials. An important caveat must be applied to these experiments, as a chromosomal deletion can result in polar effects, modifying the expression of downstream genes. An approach that may form part of future studies of antibiotic sensitivity is provided by complementation analysis of the ΔFTT1564 strain, which has potential to address this issue. Ciprofloxacin is the current antibiotic therapy of choice, according to the CDC guidelines, for the treatment of tularemia and has very effective antibiotic action against all *F. tularensis* strains [44]. Crucially, the abolition of polyphosphate production resulted in increased susceptibility to ciprofloxacin. This suggests that inhibitors of *Ft*PPK2 could act as 'antibiotic adjuvants' to enhance the efficacy of current antibiotic regimens for the treatment of tularemia, as well as acting as antibiotics in their own right. In contrast, the ΔFTT1564 mutant showed no statistically significant increase in sensitivity to polymixin B. Polymyxin B disrupts the bacterial cell membrane [45] and *F. tularensis* has known resistance; resistance is conferred by a tetra-acylated lipid A to which polymyxin B cannot bind [46]. Therefore, inactivation of polyphosphate production does not render the pathogen generally weaker due to stress, but rather the increased susceptibility is due to a specific inability to counter antibiotic killing mechanisms.

Previous studies into other Gram negative bacteria such as *P. aeruginosa*, have reported increased susceptibility to antibiotics in mutants that are defective for genes involved in the stringent response [47]. Polyphosphate production is directly influenced by the stringent response whereby abolishment of (p)ppGpp synthesis results in simultaneous decreased polyphosphate production [48]. It has also been reported that bacteria become more tolerant to antibiotics under nutrient starvation conditions [49]. That targeted mutagenesis of FTT1564 not only results in decreased polyphosphate production [17] but also in an increase in sensitivity to antibiotics, indicates that polyphosphate metabolism plays a key role in the increased antibiotic susceptibility observed upon inactivation of the stringent response.

In summary, we report the biochemical and biophysical characterization of *Ft*PPK2, an enzyme activity important for *F. tularensis* virulence [17]. The enzyme can serve as a broad specificity reversible purine diphosphate kinase, consistent with *Ft*PPK2 being the only polyphosphate kinase encoded by the *F. tularensis* genome. Inhibitors of *Ft*PPK2 could be novel antibiotics and may also enhance the activity of other antibiotics. The combined biochemical, biophysical and microbiological results reported herein, addresses some of the prerequisites for studies to discover such novel *Ft*PPK2 inhibitors.

ACCESSION CODES

The co-ordinates for *Ft*PPK2 have been deposited in the PDB with the PDB ID 4YEG.

AUTHOR CONTRIBUTION

Laura Batten, Neil Wells and Alice Parnell performed the biochemical and crystallographic experiments with *Ft*PPK2. The antibiotic sensitization experiments were performed by Amber Murch. Petra Oyston and Peter Roach designed the study and the manuscript was written through contributions of all authors.

ACKNOWLEDGEMENTS

We thank the staff and scientists at the Diamond Light Source for access to beamline i02 and help with data collection. We thank Halina Mikolajek for help with BALBES.

FUNDING

This research was supported by the Defence Threat Reduction Agency [grant number HDTRA1-11-007 (to P.L.R.)]; the Defence Science and Technology Laboratory [grant number DSTLX-1000025871 (to P.L.R.)]; and the Engineering and Physical Sciences Research Council Core Capability Funding [grant number EP/K039466/1].

REFERENCES

1 Wood, H.G. and Clark, J.E. (1988) Biological aspects of inorganic polyphosphates. Ann. Rev. Biochem. **57**, 235–260 CrossRef
2 Kornberg, A., Rao, N.N. and Ault-Riche, D. (1999) Inorganic polyphosphate: a molecule of many functions. Ann. Rev. Biochem. **68**, 89–125 CrossRef
3 Kumble, K.D. and Kornberg, A. (1995) Inorganic polyphosphate in mammalian cells and tissues. J. Biol. Chem. **270**, 5818–5822 CrossRef PubMed
4 Holmstrom, K.M., Marina, N., Baev, A.Y., Wood, N.W., Gourine, A.V. and Abramov, A.Y. (2013) Signalling properties of inorganic polyphosphate in the mammalian brain. Nat. Commun. **4**, 1362 CrossRef PubMed
5 Abramov, A.Y., Fraley, C., Diao, C.T., Winkfein, R., Colicos, M.A., Duchen, M.R., French, R.J. and Pavlov, E. (2007) Targeted polyphosphatase expression alters mitochondrial metabolism and inhibits calcium-dependent cell death. Proc. Natl. Acad. Sci. U.S.A. **104**, 18091–18096 CrossRef PubMed
6 Muller, F., Mutch, N.J., Schenk, W.A., Smith, S.A., Esterl, L., Spronk, H.M., Schmidbauer, S., Gahl, W.A., Morrissey, J.H. and Renne, T. (2009) Platelet polyphosphates are proinflammatory and procoagulant mediators *in vivo*. Cell **139**, 1143–1156 CrossRef PubMed
7 Pavlov, E., Aschar-Sobbi, R., Campanella, M., Turner, R.J., Gomez-Garcia, M.R. and Abramov, A.Y. (2010) Inorganic polyphosphate and energy metabolism in mammalian cells. J. Biol. Chem. **285**, 9420–9428 CrossRef PubMed
8 Rao, N.N., Gomez-Garcia, M.R. and Kornberg, A. (2009) Inorganic polyphosphate: essential for growth and survival. Ann. Rev. Biochem. **78**, 605–647 CrossRef
9 Rao, N.N. and Kornberg, A. (1996) Inorganic polyphosphate supports resistance and survival of stationary-phase *Escherichia coli*. J. Bacteriol. **178**, 1394–1400 PubMed
10 Wrench, A.P., Gardner, C.L., Siegel, S.D., Pagliai, F.A., Malekiha, M., Gonzalez, C.F. and Lorca, G.L. (2013) MglA/SspA complex interactions are modulated by inorganic polyphosphate. PLoS One **8**, e76428 CrossRef PubMed
11 Grillo-Puertas, M., Villegas, J.M., Rintoul, M.R. and Rapisarda, V.A. (2012) Polyphosphate degradation in stationary phase triggers biofilm formation via LuxS quorum sensing system in *Escherichia coli*. PLoS One **7**, e50368 CrossRef PubMed
12 Choi, M.Y., Wang, Y., Wong, L.L. Y., Lu, B., Chen, W., Huang, J.D., Tanner, J.A. and Watt, R.M. (2012) The two PPX-GppA homologues from *Mycobacterium tuberculosis* have distinct biochemical activities. PLoS One **7**, e42561 CrossRef PubMed
13 Tunpiboonsak, S., Mongkolrob, R., Kitudomsub, K., Thanwatanaying, P., Kiettipirodom, W., Tungboontina, Y. and Tungpradabkul, S. (2010) Role of a *Burkholderia pseudomallei* polyphosphate kinase in an oxidative stress response, motilities, and biofilm formation. J. Microbiol. **48**, 63–70 CrossRef PubMed
14 Brown, M.R. and Kornberg, A. (2008) The long and short of it - polyphosphate, PPK and bacterial survival. Trends Biochem. Sci. **33**, 284–290 CrossRef PubMed
15 Kim, K.S., Rao, N.N., Fraley, C.D. and Kornberg, A. (2002) Inorganic polyphosphate is essential for long-term survival and virulence factors in *Shigella* and *Salmonella* spp. Proc. Natl. Acad. Sci. U.S.A. **99**, 7675–7680 CrossRef PubMed
16 Hossain, M.M., Tani, C., Suzuki, T., Taguchi, F., Ezawa, T. and Ichinose, Y. (2008) Polyphosphate kinase is essential for swarming motility, tolerance to environmental stresses, and virulence in *Pseudomonas syringae* pv. tabaci 6605. Physiol. Mol. Plant Pathol. **72**, 122–127 CrossRef
17 Richards, M.I., Michell, S.L. and Oyston, P.C. (2008) An intracellularly inducible gene involved in virulence and polyphosphate production in *Francisella*. J. Med. Microbiol. **57**, 1183–1192 CrossRef PubMed
18 Shum, K.T., Lui, E.L., Wong, S.C., Yeung, P., Sam, L., Wang, Y., Watt, R.M. and Tanner, J.A. (2011) Aptamer-mediated inhibition of *Mycobacterium tuberculosis* polyphosphate kinase 2. Biochemistry **50**, 3261–3271 CrossRef PubMed
19 Whitehead, M.P., Eagles, L., Hooley, P. and Brown, M.R. (2014) Most bacteria synthesize polyphosphate by unknown mechanisms. Microbiology **160**, 829–831 CrossRef PubMed
20 Ahn, K. and Kornberg, A. (1990) Polyphosphate kinase from *Escherichia coli*. Purification and demonstration of a phosphoenzyme intermediate. J. Biol. Chem. **265**, 11734–11739 PubMed
21 Akiyama, M., Crooke, E. and Kornberg, A. (1992) The polyphosphate kinase gene of *Escherichia coli*. Isolation and sequence of the ppk gene and membrane location of the protein. J. Biol. Chem. **267**, 22556–22561 PubMed
22 Nahálka, J. and Pätoprstý, V. (2009) Enzymatic synthesis of sialylation substrates powered by a novel polyphosphate kinase (PPK3). Org. Biomol. Chem. **7**, 1778–1780 CrossRef PubMed
23 Nocek, B., Kochinyan, S., Proudfoot, M., Brown, G., Evdokimova, E., Osipiuk, J., Edwards, A.M., Savchenko, A., Joachimiak, A. and Yakunin, A.F. (2008) Polyphosphate-dependent synthesis of ATP and ADP by the family-2 polyphosphate kinases in bacteria. Proc. Natl. Acad. Sci. U.S.A. **105**, 17730–17735 CrossRef PubMed
24 Achbergerova, L. and Nahalka, J. (2014) Degradation of polyphosphates by polyphosphate kinases from *Ruegeria pomeroyi*. Biotechnol. Lett. **36**, 2029–2035 CrossRef PubMed
25 Ishige, K., Zhang, H. and Kornberg, A. (2002) Polyphosphate kinase (PPK2), a potent, polyphosphate-driven generator of GTP. Proc. Natl. Acad. Sci. U.S.A. **99**, 16684–16688 CrossRef PubMed
26 Zhang, H., Ishige, K. and Kornberg, A. (2002) A polyphosphate kinase (PPK2) widely conserved in bacteria. Proc. Natl. Acad. Sci. U.S.A. **99**, 16678–16683 CrossRef PubMed
27 Zhu, Y., Huang, W., Lee, S.S. and Xu, W. (2005) Crystal structure of a polyphosphate kinase and its implications for polyphosphate synthesis. EMBO Rep. **6**, 681–687 CrossRef PubMed

28 Leipe, D.D., Koonin, E.V. and Aravind, L. (2003) Evolution and classification of P-loop kinases and related proteins. J. Mol. Biol. **333**, 781–815 CrossRef PubMed

29 Walker, J.E., Saraste, M., Runswick, M.J. and Gay, N.J. (1982) Distantly related sequences in the alpha- and beta-subunits of ATP synthase, myosin, kinases and other ATP-requiring enzymes and a common nucleotide binding fold. EMBO J. **1**, 945–951 PubMed

30 Ellis, J., Oyston, P.C., Green, M. and Titball, R.W. (2002) Tularemia. Clin. Microbiol. Rev. **15**, 631–646 CrossRef PubMed

31 McLendon, M.K., Apicella, M.A. and Allen, L.A. (2006) *Francisella tularensis*: taxonomy, genetics, and Immunopathogenesis of a potential agent of biowarfare. Ann. Rev. Microbiol. **60**, 167–185 CrossRef

32 Rotz, L.D., Khan, A.S., Lillibridge, S.R., Ostroff, S.M. and Hughes, J.M. (2002) Public health assessment of potential biological terrorism agents. Emerg. Infect. Dis. **8**, 225–230 CrossRef PubMed

33 Winter, G., Lobley, C.M. and Prince, S.M. (2013) Decision making in xia2. Acta Crystallogr. D Biol. Crystallogr. **69**, 1260–1273 CrossRef PubMed

34 Long, F., Vagin, A.A., Young, P. and Murshudov, G.N. (2008) BALBES: a molecular-replacement pipeline. Acta Crystallogr. D Biol. Crystallogr. **64**, 125–132 CrossRef PubMed

35 Perrakis, A., Morris, R. and Lamzin, V.S. (1999) Automated protein model building combined with iterative structure refinement. Nat. Struct. Biol. **6**, 458–463 CrossRef PubMed

36 Emsley, P., Lohkamp, B., Scott, W.G. and Cowtan, K. (2010) Features and development of Coot. Acta Crystallogr. D Biol. Crystallogr. **66**, 486–501 CrossRef PubMed

37 Adams, P.D., Afonine, P.V., Bunkoczi, G., Chen, V.B., Davis, I.W., Echols, N., Headd, J.J., Hung, L.W., Kapral, G.J., Grosse-Kunstleve, R.W. et al. (2010) PHENIX: a comprehensive Python-based system for macromolecular structure solution. Acta Crystallogr. D Biol. Crystallogr. **66**, 213–221 CrossRef PubMed

38 Yount, R.G., Babcock, D., Ballantyne, W. and Ojala, D. (1971) Adenylyl imidodiphosphate, an adenosine triphosphate analog containing a P–N–P linkage. Biochemistry **10**, 2484–2489 CrossRef PubMed

39 Holm, L. and Rosenstrom, P. (2010) Dali server: conservation mapping in 3D. Nucleic Acids Res. **38**, W545–549 CrossRef PubMed

40 Leipe, D.D., Koonin, E.V. and Aravind, L. (2003) Evolution and classification of P-loop kinases and related proteins. J. Mol. Biol. **333**, 781–815 CrossRef PubMed

41 Wilson, D.N. (2014) Ribosome-targeting antibiotics and mechanisms of bacterial resistance. Nat. Rev. Microbiol. **12**, 35–48 CrossRef PubMed

42 Motomura, K., Hirota, R., Okada, M., Ikeda, T., Ishida, T. and Kuroda, A. (2014) A new subfamily of polyphosphate kinase 2 (class III PPK2) catalyzes both nucleoside monophosphate phosphorylation and nucleoside diphosphate phosphorylation. Appl. Environ. Microbiol. **80**, 2602–2608 CrossRef PubMed

43 Larsson, P., Oyston, P.C., Chain, P., Chu, M.C., Duffield, M., Fuxelius, H.H., Garcia, E., Halltorp, G., Johansson, D., Isherwood, K.E. et al. (2005) The complete genome sequence of *Francisella tularensis*, the causative agent of tularemia. Nat. Genet. **37**, 153–159 CrossRef PubMed

44 Dennis, D.T., Inglesby, T.V., Henderson, D.A., Bartlett, J.G., Ascher, M.S., Eitzen, E., Fine, A.D., Friedlander, A.M., Hauer, J., Layton, M. et al. (2001) Tularemia as a biological weapon: medical and public health management. JAMA **285**, 2763–2773 CrossRef PubMed

45 Storm, D.R., Rosenthal, K.S. and Swanson, P.E. (1977) Polymyxin and related peptide antibiotics. Ann. Rev. Biochem. **46**, 723–763 CrossRef

46 Phillips, N.J., Schilling, B., McLendon, M.K., Apicella, M.A. and Gibson, B.W. (2004) Novel modification of lipid A of *Francisella tularensis*. Infect. Immun. **72**, 5340–5348 CrossRef PubMed

47 Eng, R.H., Padberg, F.T., Smith, S.M., Tan, E.N. and Cherubin, C.E. (1991) Bactericidal effects of antibiotics on slowly growing and nongrowing bacteria. Antimicrob. Agents Chemother. **35**, 1824–1828 CrossRef PubMed

48 Candon, H.L., Allan, B.J., Fraley, C.D. and Gaynor, E.C. (2007) Polyphosphate kinase 1 Is a pathogenesis determinant in *Campylobacter jejuni*. J. Bacteriol. **189**, 8099–8108 CrossRef PubMed

49 Nguyen, D., Joshi-Datar, A., Lepine, F., Bauerle, E., Olakanmi, O., Beer, K., McKay, G., Siehnel, R., Schafhauser, J., Wang, Y. et al. (2011) Active starvation responses mediate antibiotic tolerance in biofilms and nutrient-limited bacteria. Science **334**, 982–986 CrossRef PubMed

50 Baker, N.A., Sept, D., Joseph, S., Holst, M.J. and McCammon, J.A. (2001) Electrostatics of nanosystems: application to microtubules and the ribosome. Proc. Natl. Acad. Sci. U.S.A. **98**, 10037–10041 CrossRef PubMed

Received 3 August 2015/28 September 2015; accepted 28 October 2015

Accepted Manuscript online 18 November 2015, doi 10.1042/BSR20150203